Journal of Insect Science (*2017*) 17(2): 30; 1–7
doi: 10.1093/jisesa/iew122
Research article

OXFORD

Drag Reduction in a Natural High-Frequency Swinging Micro-Articulation: Mouthparts of the Honey Bee

Guanya Shi,[1,2,*] Jianing Wu,[1,*] and Shaoze Yan[1,3]

[1]Division of Intelligent and Biomechanical Systems, State Key Laboratory of Tribology, Department of Mechanical Engineering, Tsinghua University, Beijing, People's Republic of China, [2]Department of Automotive Engineering, Tsinghua University, Beijing, People's Republic of China, and [3]Corresponding author, e-mail: yansz@mail.tsinghua.edu.cn

*These authors contributed equally to this study.

Subject Editor: Michael Heethoff

Received 11 September 2016; Editorial decision 9 November 2016

Abstract

Worker-bee mouthparts consist of the glossa, the galeae and the vestigial labial palp, and it is these structures that enable bees to feed themselves. The articulation joints, 60∼70 μm in diameter, are present on the tip of the labial palp and are covered with olfactory sensilla, allowing movements between the segments. Using a specially designed high-speed camera system, we discovered that the articulation joint could swing in the nectar at a frequency of ∼50 Hz, considerably higher than the usual motion frequency of mammalian joints. To understand the potential drag reduction in this tiny organ, we examined its microstructure and also its surface wettability. We found that chitinous semispherical protuberances (4∼6 μm in diameter) are uniformly scattered on the surface of the joint and, moreover, that the surface is hydrophobic. We proposed a hydrodynamic model and revealed that the specialized surface can effectively reduce the mean equivalent friction (F_f) by ∼10%, through the use of protuberances immersed in the liquid feed. Theoretical results indicated that the dimensions of such protuberances are the predominant factor in minimizing F_f, and that the natural dimensions of the protuberances are close to the theoretical optimum at which friction is at a minimum. These discoveries may inspire the design of high-frequency micro-joints for engineering applications, such as in micro-stirrers.

Key words: articulation, honey bee, labial palp, lubrication modelling

Introduction

Studies have revealed a myriad of morphologies and feeding strategies in insects, which have facilitated the development of next-generation products (Daniel and Kingsolver 1983, Klowden 2013). Insects offer a diverse array of anatomical variations contributing to bio-inspired technologies, and an illustrative example is the mouthparts (Kellogg 1902, Suthers 1984, Labandeira 1997, Rast and Bräunig 2001, Rogers et al. 2002). The Italian bee (*Apis mellifera ligustica*) is a typical insect for which the mouthpart morphology and function have been extensively studied (Laroca et al. 1989, Chen 2015, Wu et al. 2015, Wu et al. 2015, Zhao et al. 2015). The mouthparts of the honey bee belong to the chewing–lapping type, comprising the glossa, galeae and the vestigial labial palp, and they aid the bee in chewing pollen and lapping nectar (Dade 1994). When the bee is drinking nectar, the galeae and the labial palp form a sucking tube, within which the glossa produces a dipping motion with forward and backward movements. Current research shows that olfactory and gustatory perceptions begin at the mouthparts of a honey bee, where specific receptor neurons are located within specialized hairs, the sensilla (Whitehead 1978, Giurfa 2007, Sanchez et al. 2008). This implies that the swinging action of the joint-like articulations of the mouthparts when the mouthparts are engaged in physical activity may potentially help honey bees to capture more odor molecules for environmental perception.

In nature, the most widely-studied biological joints are the synovial joints of mammals (Woodward et al. 1969). Mammals are born with internal lubrication in their joints that increases the longevity of these joints. Furthermore, the typical mammalian joint is a cavity surrounded by tendons, ligaments and muscles, the interior of which is isolated from the external environment. Hence, the synovial fluid in the joint provides constant lubrication throughout the lifetime of the animal. In research into drag reduction in animal joints, studies focus on the rubbing of opposing bones in mammalian joints, which is mediated by layers of articular cartilage coatings that provide efficient lubrication as they slide past each other (Swann et al. 1984, Dowson and Jin 1986, Wong et al. 2008, Myant and Cann 2013).

In contrast to mammalian joints, the articulations on the tip of the honey bee's labial palp are structurally open, and are either exposed to the air or soaked in nectar, depending upon the mode of feeding (Dade 1994). Clearly, some degree of friction in joints is

inevitable when relative motion exists. However, there have apparently been no studies reported of drag reduction in open-structured micro-articulations. The labial palps of a honey bee may have a much higher frequency of motion of their tips than most mammalian limbs, and it is therefore reasonable to suppose that bees may have some special mechanisms to reduce drag and wear, thus prolonging the useful life of the micro-components. Considering the open structure of the articulation joints on the labial palp, it seems plausible that bees may use the liquid medium, typically water or nectar, as the natural source of lubricant.

In this study, we observed both the types of movement and the wettability of the specialized articulations of the labial palps of the honey bee by using a high-speed camera. Furthermore, the structural features of the uniformly-distributed protrusions on the articulation were examined using scanning electron microscopy (SEM) and transmission electron microscopy (TEM). We simulated the mechanism of drag reduction in the labial palp articulations by assuming uniformly distributed protuberances, and we hypothesize that the dimensions of the protrusions have been evolutionarily optimized.

Materials and Methods

Specimen Preparation

All the data of this study dealt with adult foraging Italian bee (*Apis mellifera Ligustica*). All specimens were collected from a single hive maintained at the intelligent bio-mechanical laboratory of Tsinghua University, Beijing, China (40.00°N, 116.32°E). The wooden beehive measured 200 mm × 300 mm × 300 mm and held a swarm of nearly 2000 Italian bees. The hive was connected to an inspection box in which we observed and captured the worker bees. The entire system was equipped with artificial ventilation to maintain the temperature at 25°C and the humidity at 50%. Twenty worker bees were selected to observe the motion of the glossa, and 10 mouthpart specimens were collected from within the wooden beehive for experimental purposes and dehydrated within 4 hours of capture. No specific permissions were required for access or collection other than our confirmation that the field studies did not involve endangered or protected species.

Observations From High-Speed Imaging

As shown in Fig. 1, the observation system consisted of a height-adjustable positioner, a sucrose channel, high-speed camera, and a light source. The observations were divided into two parts. Firstly, we filmed the bee drinking process using a high speed camera operating at 500 frames per second. In particular, we focused on the morphology of the articulations in the process of lapping nectar. Initially, the thorax of a living honey bee was fixed on the positioner using resin glue and the positioner was then lowered, allowing the honey bee's mouthparts to reach the level of the sucrose. The high-speed camera (Phantom M110, Vision Research Corporation, USA) captured the motion of the articulation joints of the labial palp in the channel filled with artificial nectar [35% wt/wt sucrose solution, which approximates the natural nectar concentration (Yang et al. 2014)]. Moreover, we measured the contact angle of the articulation statistically using the high-speed camera in time-lapse mode. Prior to the experiment, a honey bee was immersed into the ethyl alcohol and the mouthpart sample with its labial palp was used for the post-mortem test immediately. Then, we cut the labial palp from the mouthpart, and fixed it to the positioner and then we changed the height of the labial palp using the height adjuster to measure the contact angles at different vertical locations of the labial palp. We defined three parts of the labial palp (Fig. 1c) as segment III, articulation and segment IV, respectively. A computer with image-analysis software was employed to determine the tangent value precisely on the captured images.

Postmortem Examination

We used SEM (FEI Quanta 200, Czech Republic) in high-vacuum mode to observe the edge of the labial palp. Furthermore, to better understand the characteristics of the interfaces between the pin and

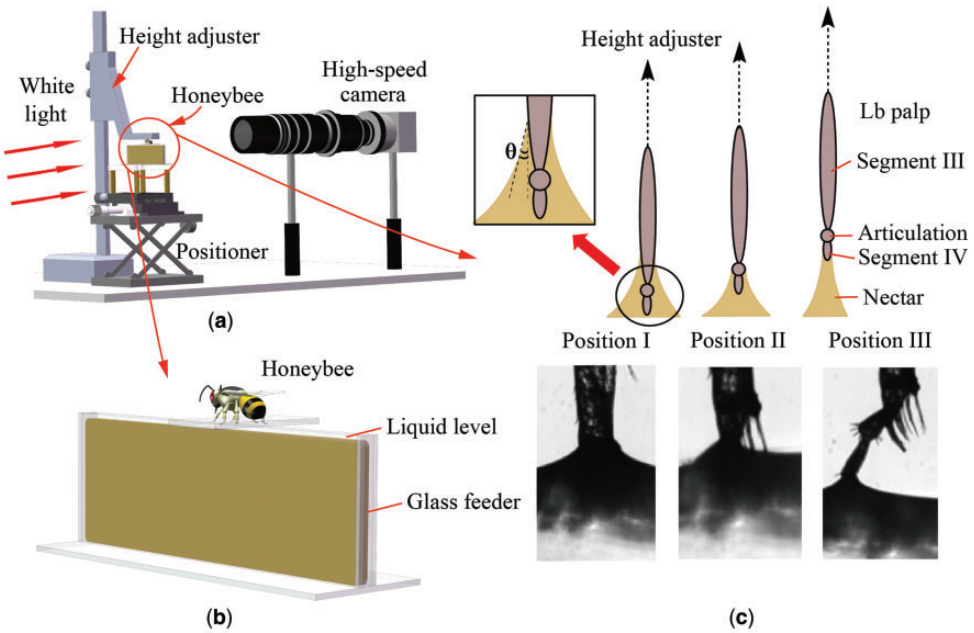

Fig. 1. Experimental setup. **(a)** The honey bee is fixed above a glass feeder illuminated by a cold light source. **(b)** The motion of the articulation is captured in the camera's field of view. **(c)** Contact angle measurement of the articulation on the labial palp. The contact angles of segment III (θ_1), articulation (θ_2) and segment IV (θ_3) are measured respectively by adjusting the height of the labial palp, and real images are also shown.

the socket, TEM (HITACHI H7650, Japan) imaging was used. To reflect the actual configurations of the joints when the tips of the labial palps were swinging in the nectar, specimens of articulation joints were captured by instantaneous freezing with liquid nitrogen when the honey bees were drinking nectar. The TEM sections were then fixed using triton (Triton X-100, Sigma-Aldrich) and resin. The depth of the cross-section of the labial palp joint is about 100 nm.

Results

Moving Kinematics and Contact Angle

We recorded the motion of the articulations in the sucrose solution, and Fig. 2 shows one cycle of the joint motion when the articulation was soaked in 35% (wt/wt) sucrose solution. The results show that the articulation joint could swing periodically in the nectar, about an axis perpendicular to the plane of Fig. 2, with a frequency of ~50 Hz, which is much higher than that of the nectar-lapping of honey bees (~5 Hz). Moreover, the contact angle of the articulation surface ($\theta_2 = 99.93°$) was much greater than that of segment III ($\theta_1 = 71.96°$) and segment IV ($\theta_3 = 37.09°$), which indicates that the articulation surface is hydrophobic. The definition of the three parts of the labial palp is shown in Fig. 1c.

Postmortem Examination Image by SEM and TEM

As indicated earlier, honey bees have typical chewing and lapping mouthparts, which can be used to eat pollen or drink nectar through alterations in their configuration (Dade 1994). As shown in Fig. 3, from SEM and TEM images, two principal discoveries were made. The first was that each labial palp has two ball-joint-like structures comprising pins and sockets to permit swinging (Fig. 3c and d). The second, of particular interest, was that hemispherical protuberances are uniformly distributed on the surface of the pin, like cobblestones (Fig. 3e–h).

Hydrodynamic Model and Drag-Reduction Mechanism

The labial palp, with many specialized hairs, sensilla, assists the glossa in sucking up nectar, and the sensilla can distinguish a large range of odors (Giurfa 2007). We captured the periodic swing (~50 Hz) of the articulation joint, which we hypothesize may benefit the olfactory and gustatory perceptions of the honey bee. Given that lubrication is essential for the articulation, the protuberances may

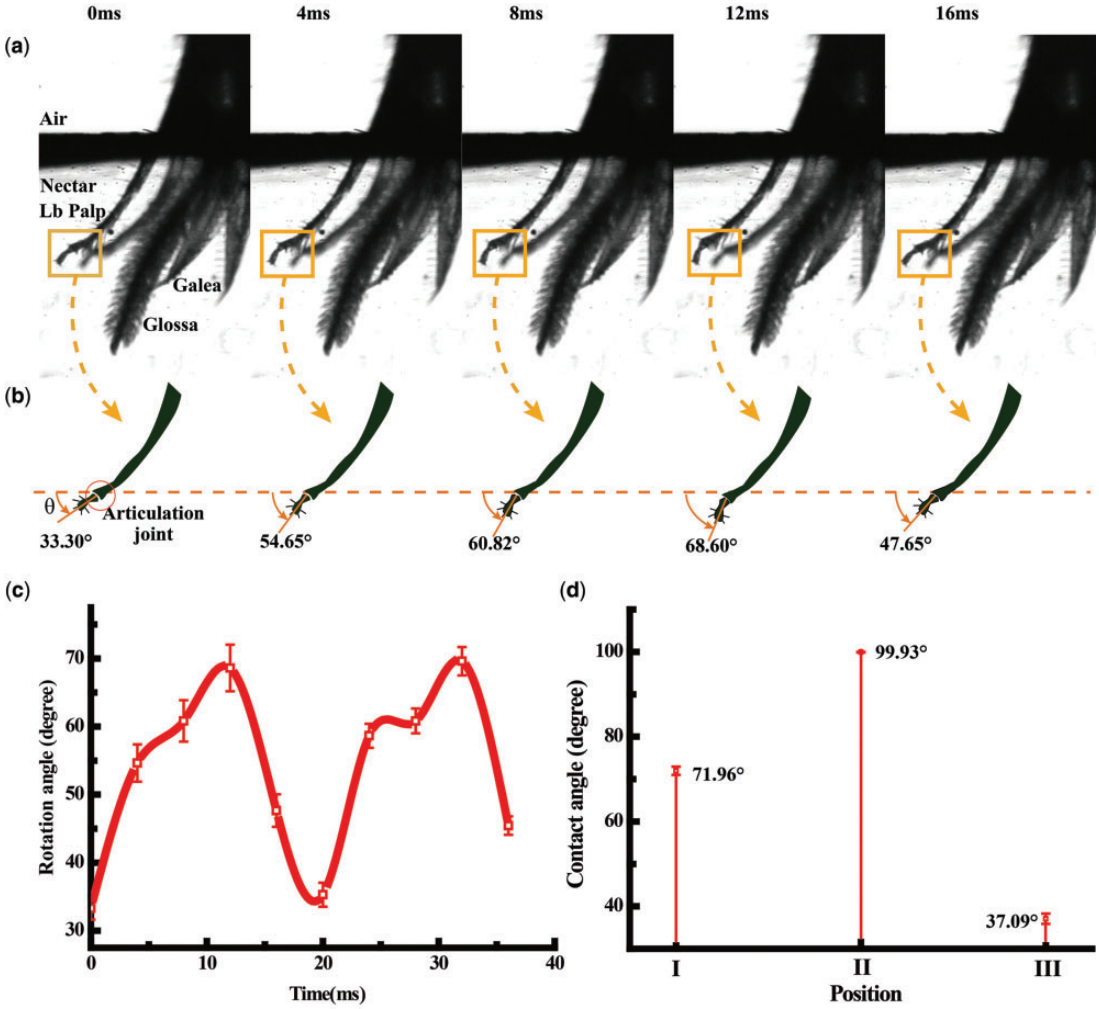

Fig. 2. Swing angles of the articulation joint and contact angles in different positions. **(a)** A cycle of frames from a high-speed movie. **(b)** Line tracings of the labial palp joint movements; the labial palp is shown in dark green. The articulation joint of the honey bee reciprocates when the bee is drinking nectar. **(c)** The movement profile of the articulation's swing in two cycles. The cycle of joint swinging is about 20 ms and the angle ranges from 33.3° to 69.6°. **(d)** The contact angle of Positions I~III (Fig. 1c). Average values of the contact angles in Positions I~III are 71.96°, 99.93° and 37.09°, respectively.

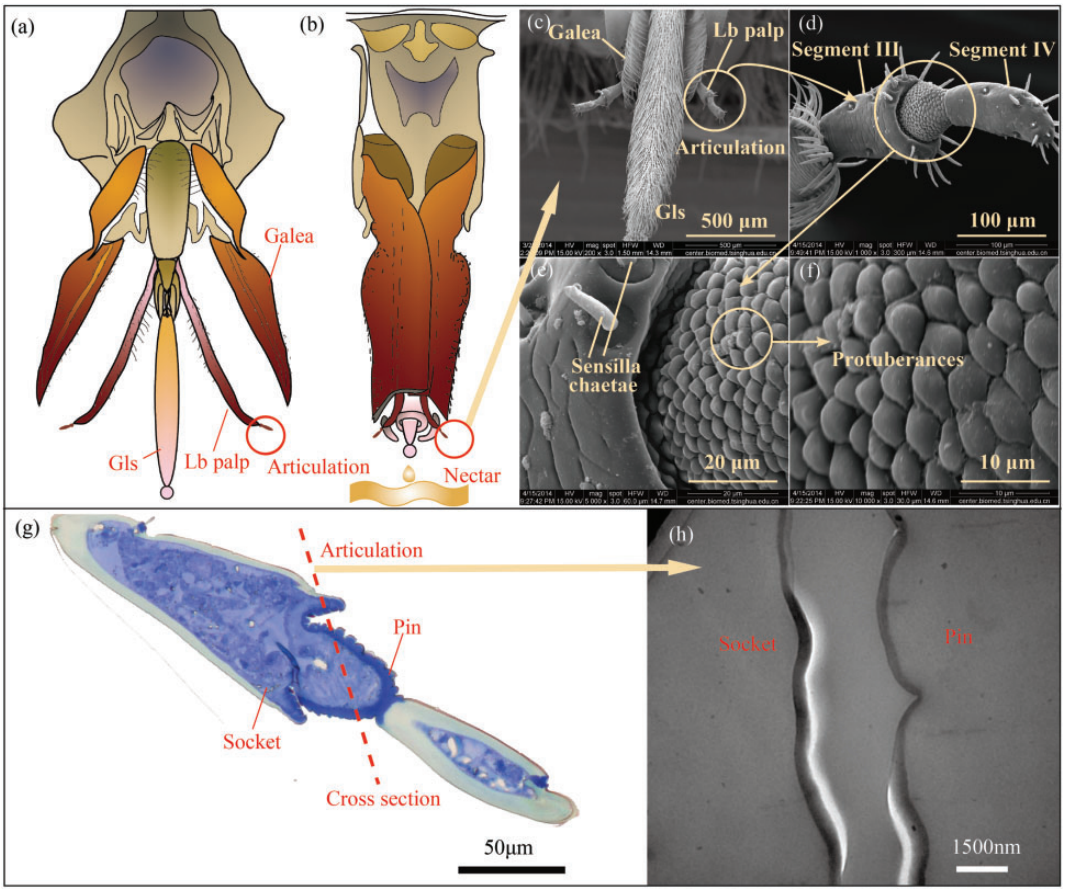

Fig. 3. Structural features of the mouthparts of the worker honey bee. To ensure measurement precision and repeatability, 10 specimens were analyzed. **(a)** The mouthparts comprise the galeae, labial palp and the glossa. **(b)** When the honey bee is ready to imbibe liquid food, the galeae and labial palp are brought closely together to form a tube around the glossa, a sucking tube, which is similar to a drinking-straw. **(c)** SEM image of the mouthparts. **(d)** We observed the edge of the labial palp and found that two ball-joint-like articulations of 60∼70 μm in diameter were attached. The ball-joint-like structure comprises the pin and socket by which the ball joint can swing. **(e)-(f)** In the partially magnified image, we discovered that 4∼6 μm semispherical protuberances were uniformly distributed on the surface of the pin. **(g)** Longitudinal slice of the labial palp stained with toluidine blue, in which the two parts of the structure, the socket and the pin, are named. **(h)** The TEM image.

help to reduce drag and friction. In analyzing the lubrication effect of this specialized structure, we proposed a hydrodynamic model of Reynolds blocks and considered the protuberances according to Reynolds equations (Li et al. 2016).

We focused on one cross-section of the labial palp only, as shown in Fig. 4a, and therefore this hydrodynamic model was simplified as a typical 2D one. Given that the radius of the pin is ∼100 times the width of the clearance between the pin and the socket, and that the diameter of each protuberance is around 1% of the diameter of the pin, we used a local coordinate system for the surface of the socket, as shown in Fig. 4c. We defined ω as the constant swing frequency of the pin (Fig. 4b), which was calculated according to our high-speed camera recordings, and u as the translation velocity (Fig. 4c).

After fitting the shape of the protuberance (Fig. 4c), we have

$$h = \begin{cases} h_0 e^{-ax}, 0 \le x < R \\ h_0 e^{a(x-2R)}, R \le x < 2R \end{cases} \quad (1)$$

where a, h_0, R are three geometrical parameters of the protuberance, and $h(x)$ is the distance between the protuberance and the socket. The size of the protuberance increases as R increases and the degree of bluntness of the protuberance increases as a increases. Twenty protuberances were selected to be fitted as per Eq. (1), and the average goodness of fit was 0.96.

We regarded the protuberances on the pin as Reynolds blocks, and the Reynolds Equation for such protrusions can be expressed as

$$\frac{d}{dx}\left(h^3 \frac{dP}{dx}\right) = -6\eta u \frac{dh}{dx} \quad (2)$$

where $P(x)$ is the pressure, and η is the viscosity of the sucrose solution.

Note that $\frac{dh}{dx} = -ah(0 \le x < R), \frac{dh}{dx} = ah(R \le x < 2R)$, and the pressures at points A, B and C are P_{i-1}, P_i, P_{i+1}, respectively. We can therefore obtain the following equations by solving Eqs. (1) and (2)

$$P = \begin{cases} -\frac{3\eta u}{ah^2} + C_1 \frac{1}{3ah^3} + C_2, 0 \le x < R \\ \frac{3\eta u}{ah^2} - C_3 \frac{1}{3ah^3} + C_4, R \le x < 2R \end{cases} \quad (3)$$

in which

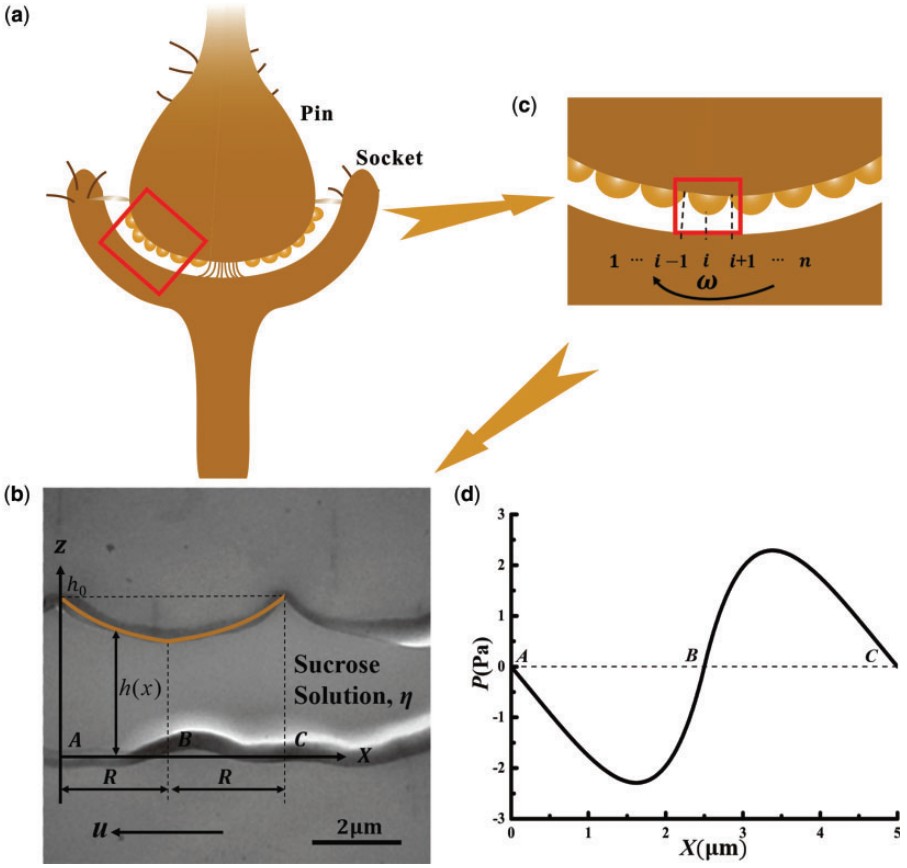

Fig. 4. Physical model of the lubrication mechanism of the special joint structure. **(a)** Model of the articulation. **(b)** The partially magnified image of the articulation model. **(c)** The shape of the protuberance on the pin is fitted from the TEM image. **(d)** The pressure *P* of the clearance against the horizontal distance *X*.

$$\begin{cases} C_1 = \dfrac{9\eta u h_0(e^{2aR}-1)+3ah_o^3(P_i-P_{i-1})}{e^{3aR}-1} \\ C_2 = \dfrac{3\eta u(e^{3aR}-e^{2aR})}{ah_0^2(e^{3aR}-1)}+\dfrac{e^{3aR}P_{i-1}-P_i}{e^{3aR}-1} \\ C_3 = \dfrac{9\eta u h_0(e^{2aR}-1)+3ah_o^3(P_{i+1}-P_i)}{e^{3aR}-1} \\ C_4 = -\dfrac{3\eta u(e^{3aR}-e^{2aR})}{ah_0^2(e^{3aR}-1)}+\dfrac{e^{3aR}P_{i+1}-P_i}{e^{3aR}-1} \end{cases} \quad (4)$$

The flow of sucrose solution in the gap between the pin and the socket should satisfy the motion equations (Bhushan 2013). Moreover, to preserve the mass conservation in the given system, we set the left and right surfaces as the velocity inlet boundary and the outflow boundary, respectively. In addition, we speculate that the protuberances are distributed uniformly on the pin. The speed $u(z)$ can be described as

$$u(z) = \frac{1}{2\eta}\frac{dP}{dx}\left(z^2 - zh\right) + \frac{uz}{h} - u \quad (5)$$

and unit discharge (the unit volume rate of flow) denotes

$$q(x) = \int_0^{h(x)} u(z)dz \quad (6)$$

After integration, we obtain

$$q(x) = \begin{cases} \dfrac{-C_1}{12\eta}, 0 \le x < R \\ \dfrac{-C_3}{12\eta}, R \le x < 2R \end{cases} \quad (7)$$

Depending on the theory of continuous flow (Fig. 4b) (Hori 2006), we have

$$q_{x(i-1)} = q_{xi} = q_{x(i+1)} \quad (8)$$

since $C_1 = C_3$, and we have $P_i - P_{i-1} = P_{i+1} - P_i$.

Now we consider all the protuberances on the pin (Fig. 4b). Similarly, with the boundary conditions $P_1 = P_n = 0$, all pressures can be expressed by

$$\begin{cases} P_{i-1} - Pi - 2 = P_i - P_{i-1} (i = 3, 4, \ldots, n) \\ P_1 = P_n = 0 \end{cases} \quad (9)$$

By solving Eq. (9), we have $P_1 = P_2 = \ldots = P_n = 0$, which means that all the protuberances have the same boundary conditions. By estimating the dimensions from SEM and TEM images, we can predict three geometry parameters a, h_0, and R (Fig. 4c). In addition, the fluid viscosity η rises sharply when the sucrose concentration is increased, which can be fitted by

$$\eta(\mathrm{s}) = \frac{10^{0.8752s/(100-s)+s^2/9901}}{1009.7} \quad (10)$$

when the temperature is 25°C (Pivnick and McNeil 1985).

Based on the above equations and the flow behavior of sucrose solution, we obtain the mapping of pressure P against X for each protuberance, shown in Fig. 4d. All the variables for calculating the pressure are presented in Table 1.

The gap filled with nectar can separate the socket and the pin from each other, which generates an effective lubrication. To better

understand the mechanism of lubrication, we propose a mean equivalent friction F_f of protuberances to evaluate the drag, which reads

$$F_f = \frac{F}{l} \tag{11}$$

where l is the length of protuberance curves, which is

$$l = 2\int_0^R \sqrt{1 + h_0^2 a^2 e^{-2ax}}\,dx \tag{12}$$

and F is the summation of the friction, which can be calculated as

$$F = \int_0^{2R} \tau|_{z=h}\,dx = \int_0^{2R} \eta \frac{\partial u}{\partial z}|_{z=h}\,dx = \int_0^{2R} \frac{1}{2}\frac{dP}{dx}h\,dx + \int_0^{2R} \eta\frac{u}{h}\,dx \tag{13}$$

based on the vertical distribution of speed in Eq. (5). With Eq. (3) and boundary conditions in Eq. (9), we finally obtain

$$F = -\frac{\eta u}{h_0}\frac{e^{aR}-1}{a} + \frac{3\eta u}{2h_0}\frac{(e^{2aR}-1)^2}{a(e^{3aR}-1)} + \frac{3\eta u}{h_0}\frac{(e^{aR}-1)(e^{2aR}-e^{3aR})}{ae^{aR}(e^{3aR}-1)} \tag{14}$$

Table 1. Parameters for calculating the pressure for each protuberance

Parameter	Value	Unit
u	2.2×10^{-3}	$m \cdot s^{-1}$
R	2.5×10^{-6}	m
h_0	3.3×10^{-6}	m
a	3.0×10^{5}	m^{-1}
η	3.9×10^{-3}	$Pa \cdot s$

By using Matlab R2014a (MathWorks, Natick, MA, USA), we calculated the dependence between F_f and the three geometrical parameters, namely a, R, and h_0. We found that under different values of R, F_f first increases slightly as a increases, and then F_f decreases to a minimum. Subsequently, F_f increases markedly as the geometrical parameter a increases further. Thus, there is an optimal value of a for each given value of R, leading to a great reduction in F_f when other parameters (h_0, η, and u) are set as fixed. Results for the variation of F_f against a for different values of R are illustrated graphically in Fig. 5.

We can distinguish at least two intrinsic links between F_f and the geometrical parameters. First, we found that F_f decreases as R decreases. Optimization of geometrical parameter a under $R = 1.9$, 2.2, 2.5, and 2.8 μm can reduce F_f to 2.26, 2.48, 2.66, and 2.81 N/m^2, respectively, and the value of F_f without protuberances is 2.67 N/m^2. This indicates that a higher distribution density of protuberances for a fixed surface area contributes more to reducing the fluidic drag, and specifically, much smaller protuberances are beneficial in drag reduction. Secondly, when we focus on the inlet in Fig. 5 that describes the geometry of one protuberance under the criterion of optimal F_f, we find that the optimal value for a decreases when we select a larger value for R. Under $R = 1.9$, 2.2, 2.5, and 2.8 μm, the optimal geometry parameter a is equal to 0.88, 0.74, 0.62, and 0.52 μm^{-1}, respectively, which means that the degree of bluntness for optimal shape decreases when R increases, as shown by the optimal shape for each value of R in Fig. 5. We define the height of protuberance as $H = h_0(1 - e^{-K})$, where $K = aR$ (Fig. 5). It can be concluded that under different values of R, the optimal value for K in contributing to drag reduction is 1.58 ± 0.09, which means that the optimal height, H, of protuberance under different values of R is consistent, and that H is a key factor in reducing drag. Moreover, from the orange shading in Fig. 5, we found that the scattered experimental results are close to the theoretically-optimal ones, and that

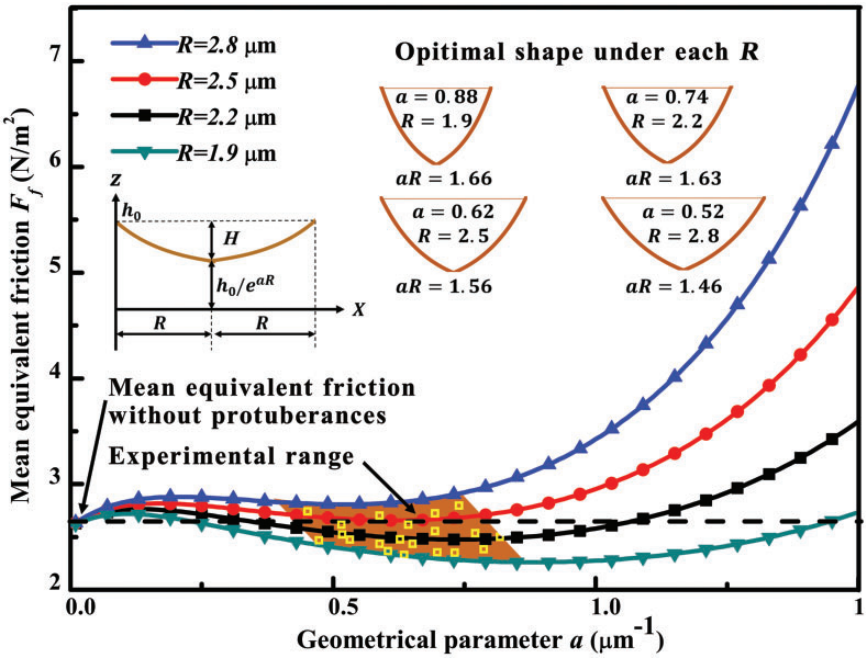

Fig. 5. Mapping of mean equivalent friction F_f against the geometrical parameter a under different values of R (1.9, 2.2, 2.5, and 2.8 μm). The mean equivalent friction F_f on the pin–nectar interface with no protuberances ($a = 0$) is represented in the dashed line (2.67 N/m^2). In addition, we measured a and R of the protuberances based on the SEM images and then calculated F_f according to Equations (11)–(14); the results are presented in yellow squares scattered in the orange region ($n = 20$ protuberances).

the average reduction in F_f is 9.6% compared to F_f without protuberances ($n = 20$ protuberances).

Discussion

According to the analyses above, the presence of protuberance microstructure on the pin of the articulating joint helped to reduce drag and friction. Furthermore, during the feeding of honey bees, sugar water may be enabled to detach more rapidly from the liquid–solid interface on account of the low friction between the droplet and the hydrophobic substrate (Liu et al. 2015). Consequently, the hydrophobic surface with protuberances remains clean, which enhances the adaptability of the honey bee to a variety of feeding circumstances.

Equipped with chewing and lapping mouthparts, honey bees could be considered as optimal foragers. In contrast to mammals, honey bees use natural lubricants, to ensure the adaptability of the micro-articulation mechanism under different feeding conditions. In this study, we captured the honey bee feeding process using a high-speed camera, and detected the high-frequency swinging and hydrophobic surfaces of the articulation joints of the labial palp. The microstructural features of the articulation were observed in SEM and TEM images. In the light of these observations, a physical model was proposed to analyze the lubrication mechanism of the articulation joints by considering in particular the protuberances on the joint pin. The results demonstrate that honey bees have evolved a highly-specialized form of lubrication that prolongs the service life of the micro-articulation and enhances the adaptability and viability of honey bees under various different environmental conditions. Finally, the lubrication mechanism in these natural micro-joints may inspire the design of next-generation miniature hinges for use in micro-blenders and micro-stirrers for biochemical reactions, since all these micro devices usually rotate or swing in viscous fluid, through micro-articulations.

Acknowledgments

We are grateful to the Centre of Biomedical Analysis of Tsinghua University for their assistance with the specimen processing and SEM image capturing. This study was funded by the National Natural Science Founding of China (Grant 51475258) and a Research Project of the State Key Laboratory of Tribology (Grant SKLT11B03).

References Cited

Bhushan, B. 2013. Introduction to tribology, 2nd ed. Wiley, New York, USA.

Chen, J. 2015. Switchable wettability of the honeybee's tongue surface regulated by erectable glossal hairs. J. Insect. Sci. 15: 164.

Dade, H. A. 1994. Anatomy and dissection of the honeybee. International Bee Research Association, Bristol, UK.

Daniel, T. L., and J. G. Kingsolver. 1983. Feeding strategy and the mechanics of blood sucking in insects. J. Theor. Biol. 105: 661–672.

Dowson, D., and Z. M. Jin. 1986. Micro-elastohydrodynamic lubrication of synovial joints. Eng. Med. 15: 63–65.

Giurfa, M. 2007. Behavioral and neural analysis of associative learning in the honeybee: a taste from the magic well. J. Comp. Physiol. A. 193: 801–824.

Hori, Y. 2006. Hydrodynamic lubrication. Springer, Berlin, Germany.

Kellogg, V. L. 1902. The development and homologies of the mouth parts of insects. Am. Nat. 36: 683–706.

Klowden, M. J. 2013. Physiological systems in insects. Academic Press, Cambridge, USA.

Labandeira, C. C. 1997. Insect mouthparts: ascertaining the paleobiology of insect feeding strategies. Annu. Rev. Ecol. Syst. 28: 153–193.

Laroca, S., C. D. Michener, and R. M. Hofmeister. 1989. Long mouthparts among "short-tongued" bees and the fine structure of the labium in Niltonia (Hymenoptera, Colletidae). J. Kansas Entomol. Soc. 62: 400–410.

Li, C., J. Wu, Y. Yang, R. Zhu, and S. Yan. 2016. Drag reduction effects facilitated by microridges inside the mouthparts of honeybee workers and drones. J. Theor. Biol. 389: 1–10.

Liu, Y., M. Andrew, J. Li, J. M. Yeomans, and Z. Wang. 2015. Symmetry breaking in drop bouncing on curved surfaces. Nat. Commun. 6: 100034.

Myant, C., and P. Cann. 2013. In contact observation of model synovial fluid lubricating mechanisms. Tribol. Int. 63: 97–104.

Pivnick, K. A., and J. N. McNeil. 1985. Effects of nectar concentration on butterfly feeding: measured feeding rates for *Thymelicus lineola* (Lepidoptera: Hesperiidae) and a general feeding model for adult Lepidoptera. Oecologia 66: 226–237.

Rast, G. F., and P. Bräunig. 2001. Insect mouthpart motor patterns: central circuits modified for highly derived appendages. Neuroscience 108: 167–176.

Rogers, B. T., M. D. Peterson, and T. C. Kaufman. 2002. The development and evolution of insect mouthparts as revealed by the expression patterns of gnathocephalic genes. Evol. Dev. 4: 96–110.

Sanchez, M. G d B., C. Chen, J. Li, F. Liu, M. Gauthier, and M. Giurfa. 2008. Behavioral studies on tarsal gustation in honeybees: sucrose responsiveness and sucrose-mediated olfactory conditioning. J. Comp. Physiol. A. 194: 861–869.

Suthers, I. M.1984. Functional morphology of the mouthparts and gastric mill in *Penaeus plebejus* Hess (Decapoda: Penaeidea). Mar. Freshwater. Res. 35: 785–792.

Swann, D. A., K. J. Bloch, D. Swindell, and E. Shore. 1984. The lubricating activity of human synovial fluids. Arthritis. Rheum-US. 27: 552–556.

Whitehead, A. T. 1978. Electrophysiological response of honeybee labial palp contact chemoreceptors to sugars and electrolytes. Physiol. Entomol. 3: 241–248.

Wong, B. L., W. C. Bae, J. Chun, K. R. Gratz, M. Lotz, and R. L. Sah. 2008. Biomechanics of cartilage articulation: effects of lubrication and degeneration on shear deformation. Arthritis. Rheum-US. 58: 2065–2074.

Woodward, D. H., A. Gryfe, and D. L. Gardner. 1969. Comparative study by scanning electron microscopy of synovial surfaces of four mammalian species. Experientia 25: 1301–1303.

Wu, J., H. Yang, and S. Yan. 2015. Energy saving strategies of honeybees in dipping nectar. Sci. Rep-UK. 5: 15002.

Wu, J., R. Zhu, S. Yan, and Y. Yang. 2015. Erection pattern and section-wise wettability of honeybee glossal hairs in nectar feeding. J. Exp. Biol. 218: 664–667.

Yang, H., J. Wu, and S. Yan. 2014. Effects of erectable glossal hairs on a honeybee's nectar-drinking strategy. Appl. Phys. Lett. 104: 263701.

Zhao, C., J. Wu, and S. Yan. 2015. Observation and temporal model of a honeybee's hairy tongue in microfluid transport. J. Appl. Phys. 118: 194701.